Fluid Controls on Ore Genesis in the Eskay Creek Deposit, Northwestern British Columbia (NTS 104B/09, /10)

T. Meuzelaar, Department of Geology and Geological Engineering, Colorado School of Mines, Golden CO, tmeuzela@mymail.mines.edu

T. Monecke, Department of Geology and Geological Engineering, Colorado School of Mines, Golden CO

Meuzelaar, T. and Monecke, T. (2012): Fluid controls on ore genesis in the Eskay Creek deposit, northwestern British Columbia (NTS 104B/09, /10); *in* Geoscience BC Summary of Activities 2011, Geoscience BC, Report 2012-1, p. 41–52.

Abstract

Geochemical modelling was performed to constrain fluid controls on the formation of the Eskay Creek sulphide and sulphosalt deposit in northwestern British Columbia. Using recently published H_2S solubility data, models of seafloor sulphide precipitation were developed for several modern seafloor vents of known fluid compositions. The modelling suggests that a fluid with a pH of 4.5–5.0 could have precipitated sphalerite at Eskay Creek at temperatures of 180–220ºC. Such a fluid could have sufficient alkalinity to reach carbonate saturation, which is required to explain the origin of the carbonate-kaolinite alteration in the mudstone hosting the stratiform orebodies of clastic sulphide and sulphosalt deposits. The geochemical modelling demonstrates that the Eskay Creek deposit formed from a near-neutral and relatively reducing fluid. As the chemical character of the hydrothermal fluid is not unusual for submarine hydrothermal systems, exploration for volcanic-hosted, precious-metal deposits such as Eskay Creek can be guided by criteria not unlike those used in the search for conventional massive sulphide deposits.

Purpose of Research

The Eskay Creek deposit (MINFILE 104B 008; BC Geological Survey, 2011) in northwestern BC represents an unusual volcanic-hosted sulphide and sulphosalt deposit that is characterized by high precious-metal concentrations (average of 48.4 g/t Au and 132.2 g/t Ag), a geochemical association of the precious metals with the epithermal suite of elements, and low temperatures (<200°C) of sulphide and sulphosalt deposition (Roth et al., 1999). Based on these deposit attributes, Eskay Creek is considered to represent the type example of a new group of volcanic-hosted gold deposits that formed in relatively shallow water, submarine environments, where phase separation of the hydrothermal fluids represented an important control on metal precipitation (Hannington et al., 1999).

Detailed mineralogical and geochemical investigations of the hostrocks of the Eskay Creek deposit resulted in the definition of a distinctive alteration halo surrounding the deposit (Ettlinger, 1992; Roth et al., 1999; Meuzelaar and Monecke, 2011). Most notable is an extensive zone of carbonate-kaolinite alteration in the carbonaceous mudstone hosting the stratiform clastic sulphide and sulphosalt orebodies. This style of alteration is largely restricted to areas overlying upflow zones of mineralizing hydrothermal fluids and associated discordant sulphide zones in the footwall rhyolite. The newly defined alteration signature and compositional trends within the carbonaceous mudstone can be used to parameterize models of fluid evolution aimed at understanding deposit genesis and the unique geochemical footprint of the Eskay Creek deposit.

Previous numerical simulations of submarine ore-forming processes have so far been impaired by a number of issues, including the quality of H_2S-solubility data in databases used for geochemical modelling. In this paper, it is shown that the data from Duan et al. (2007) provide reliable constraints on H_2S solubility. The quality of the data was tested by modelling sulphide precipitation at modern seafloor vent sites, where the compositions of the mineralizing chloride waters are known. The results indicate that predicted sulphide-precipitation temperatures are in agreement with seafloor observations. Based on published homogenization temperatures of fluid inclusions in sphalerite, it is possible for the first time to constrain the chemical nature of the fluids responsible for the formation of the Eskay Creek deposit. The findings of the geochemical modelling have significant implications for exploration as they show that gold-rich massive sulphide deposits, such as the Eskay Creek deposit, are not formed by hydrothermal fluids of unusual chemical character.

Geology

The Eskay Creek deposit is located on the western margin of the allochthonous Stikine terrane of the northern Cana-

Keywords: *Eskay Creek deposit, massive sulphide deposits, gold, ore vectors, H_2S solubility, sulphide precipitation, geochemical modelling*

This publication is also available, free of charge, as colour digital files in Adobe Acrobat® PDF format from the Geoscience BC website: http://www.geosciencebc.com/s/DataReleases.asp.

dian Cordillera (Figure 1). The hostrock succession of the deposit is part of the Upper Hazelton Group, which formed by extensional, continental-margin arc volcanism between 181 and 172 Ma (Barrett and Sherlock, 1996; Childe, 1996).

The hostrocks of the deposit are folded into a shallowly north-plunging, north-northeast-trending, upright open anticline (Figure 1). The ore zones of the Eskay Creek deposit occur on the western limb of the fold, near the fold closure, and dip gently 30–45° to the west. The metamorphic grade in the mine area is lower greenschist (Roth et al., 1999). The bulk of the mineralization consists of stratiform clastic beds and laminations of commonly graded sulphide and sulphosalt debris, which are hosted by a thick interval of carbonaceous mudstone at the contact between felsic volcanic rocks and overlying basalt (Britton et al., 1990; Ettlinger, 1992). In addition to the stratiform orebodies, economic concentrations of precious metals have been recognized in discordant zones of sulphide veins and disseminations in the footwall rhyolite.

The stratigraphic footwall of the deposit is composed of multiple rhyolite units and associated volcaniclastic deposits, reaching a maximum apparent thickness of approximately 100 m in the mine area (Britton et al., 1990). Hydrothermal alteration is widespread throughout the footwall rhyolite (Robinson, 1991; Barrett and Sherlock, 1996). Secondary potassium-feldspar formation and moderate silicification occurred in the periphery of the stratiform ores and in deeper parts of the footwall. Immediately underlying the stratiform ore zones, a tabular zone of more intense and texturally destructive chlorite and white mica alteration is recognized (Ettlinger, 1992; Roth et al., 1999). An unusual hydrocarbon alteration occurs locally below the stratiform ore zones (Ettlinger, 1992; Barrett and Sherlock, 1996; Roth et al., 1999).

The footwall rhyolite is overlain by carbonaceous mudstone, which hosts the stratiform ore zones of clastic sulphide and sulphosalt deposits. The carbonaceous mudstone has an apparent stratigraphic thickness that ranges from <1 to >60 m (Britton et al., 1990); it is laminated, thinly bedded or massive and contains abundant intercalated, tan-coloured beds of fine-grained volcaniclastic material. Calcareous and siliceous intervals are present, but not common. The carbon content generally decreases toward the top of the unit. The mudstone contains radiolarians, dinoflagellates, rare belemnites and corals, suggesting a marine depositional environment (Britton et al., 1990; Robinson,

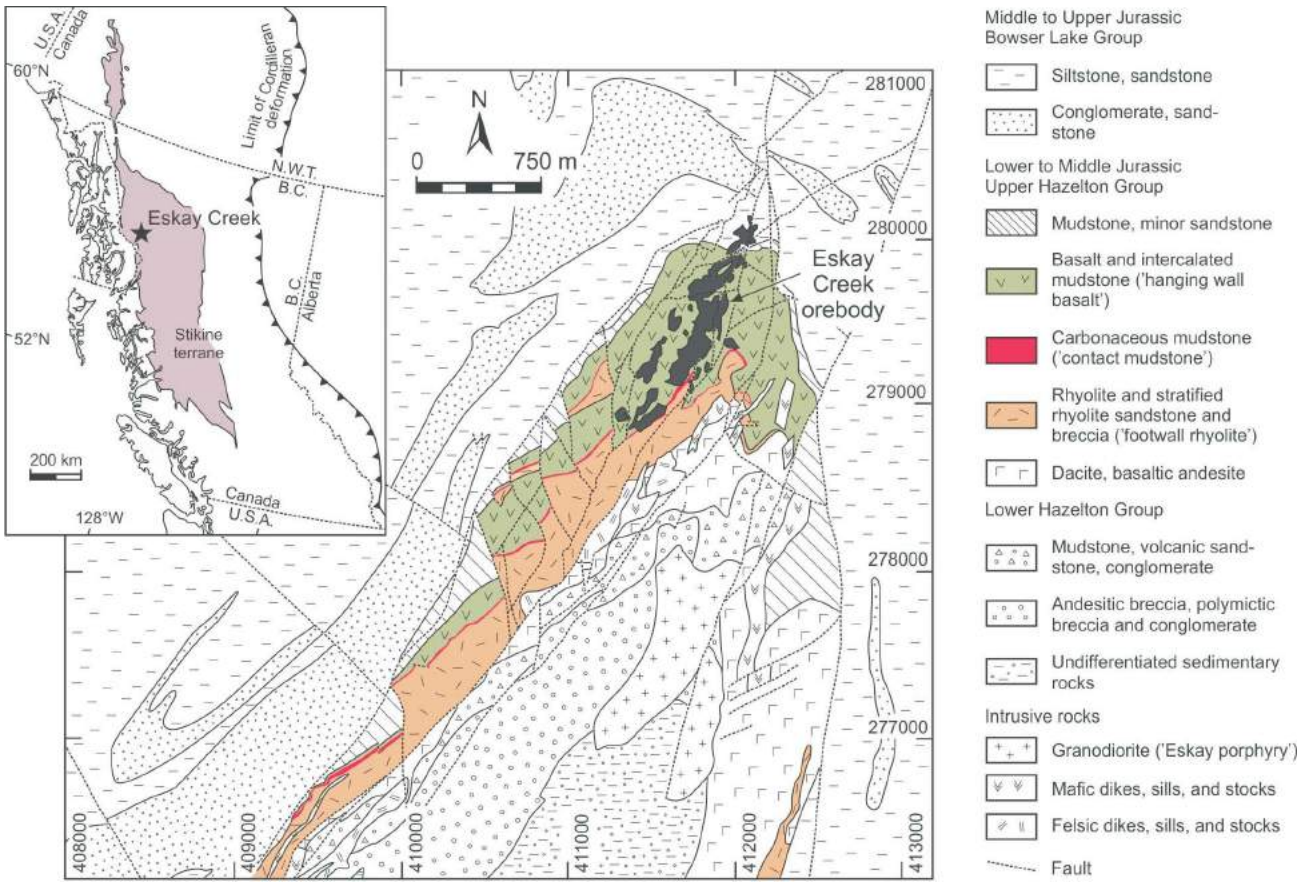

Figure 1. Geology of the Eskay Creek anticline, showing the location of the surface projection of the ore zones (modified from Alldrick et al., 2005). Inset shows the location of the deposit in the Stikine terrane (modified from Gabrielse et al., 1991).

1991; Nadaraju, 1993; Monecke et al., 2005). Thin pyrite laminations are common throughout the unit. The occurrence of flame structures at the base of the sulphide laminations indicates that the pyrite is clastic in origin (Britton et al., 1990; Monecke et al., 2005). In addition to the sulphide laminations, thin veins and veinlets of pyrite crosscutting bedding are widespread close to the contact with the underlying rhyolite.

Basalt sills and dikes occur throughout the carbonaceous mudstone unit. The occurrence of mudstone-matrix basalt breccia along the bottom and top margins of coherent basalt intervals indicates that the lava intruded the mudstone when it was still wet and unconsolidated (Monecke et al., 2005). The relative proportion of basalt increases in the upper part of the hostrock succession of the Eskay Creek deposit. Both intrusive and extrusive basalt units occur at this stratigraphic level, forming an interval up to 150 m thick, which generally thins southward, away from the deposit (Britton et al., 1990).

Previous work

Results of a detailed mineralogical and geochemical study of the carbonaceous mudstone hosting the Eskay Creek deposit (Meuzelaar and Monecke, 2011) revealed a number of important geochemical trends, which can be used both for numerical-model parameterization and target vectoring when exploring for precious and base metals. The occurrence of carbonate minerals appears to correlate with the distance to the mineralized zones, with higher dolomite-ankerite and magnesite-siderite abundances indicating proximity to the ore zones at the base of the mudstone unit. Magnesian calcite is abundant in the stratigraphic hanging-wall proximal to the stratiform ore zones.

In addition to carbonate alteration, which appears to be the most reliable vector of proximity within tens to hundreds of metres of mineralized zones, the composition of chlorite appears to vary systematically. Chlorite close to mineralization is characterized by an increased Mg content, which is consistent with compositional trends observed in the carbonate mineralogy. Local silicification of mudstone has been noted. Strongly altered mudstone samples collected close to the upflow zones of hydrothermal fluids are characterized by Na_2O depletion, which is caused by feldspar-destructive alteration commonly associated with submarine sulphide mineralization (e.g., Large, 1977; Schardt et al., 2001). Proximity to mineralization is also reflected in elevated F contents in sheet silicates, systematic changes in the Cs/Rb ratio of white mica and the Ni/V ratio in organic carbon.

The mudstone samples show increases in the galena, chalcopyrite and sphalerite contents with proximity to ore. Pyrite contained in background mudstone samples is mostly of diagenetic origin. However, pyrite that is distinctly enriched in As has also been recognized This type of pyrite is interpreted to have formed in association with the sulphide and sulphosalt mineralization. Mineralogical variations in the mudstone samples in proximity to ore are reflected by increased Ag, As, Au, Cd, Cu, Sb, Pb, Te and Zn concentrations in whole-rock geochemical analyses. There is a strong correlation between the precious- and base-metal contents of the carbonaceous mudstone, which is reflective of the overall metal signature of the Eskay Creek deposit.

H_2S Solubility

Numerical simulation of the ore-forming processes at Eskay Creek and of those responsible for the formation of the associated carbonate-kaolinite alteration halo requires an adequate description of the H_2S solubility in the hydrothermal fluids.

Duan et al. (2007) summarized the results of previous experimental investigations, which have thus far been conducted only under a comparably narrow range of temperatures, pressures and salinities. Duan et al. (2007) also discussed the limitations of the various experimental studies and proposed a new thermodynamic model calculating the H_2S solubility in pure water and aqueous NaCl solutions. The model calculates the chemical potential of H_2S in the vapour phase using the equation of state presented in Duan et al. (1996), whereas the chemical potential of H_2S in the liquid phase is modelled using the approach described by Pitzer (1973). The proposed model is valid for solutions of varied electrolyte compositions, with ionic strengths (measured in terms of the NaCl molality) of 0–6 molal, at temperatures of 0–227°C, and H_2S fugacities of 0–200 bar (an online solubility calculator is available at http://calc.geochem-model.org/).

To conduct modelling for the present study, the H_2S-solubility data of Duan et al. (2007) was initially used to calculate the equilibrium constant K for the reaction and the corresponding mass-action equation

$$H_2S(aq) = H_2S(g)$$

$$K = f[H_2S(g)]/a[H_2S(aq)] \quad (1)$$

where f is the fugacity of the gas and a is the activity of H_2S in the solution. The fugacity of H_2S as a gas and the activity of H_2S in solution were made dimensionless based on the choice of an appropriate standard state (Bethke, 2008).

The values of the equilibrium-constant K for different temperatures calculated this way were inserted into the Lawrence Livermore National Laboratory (LLNL) thermochemical database (Delany and Lundeen, 1990), replacing the equilibrium constants originally given in the database. The original equilibrium constants for the LLNL and the extended LLNL thermochemical databases at temperatures ranging from 0 to 300ºC are given in Figure 2.

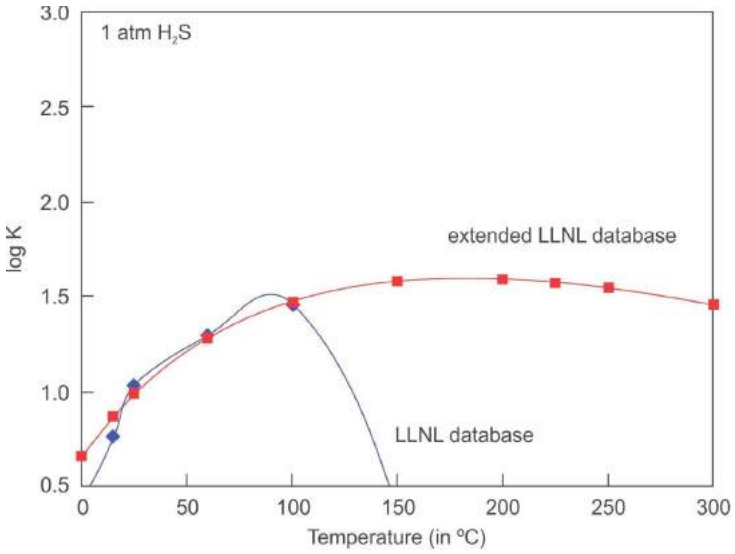

Figure 2. Temperature dependency of the equilibrium-constant K for the reaction $H_2S(aq) = H_2S(g)$, according to the Lawrence Livermore National Laboratory (LLNL) thermochemical database (Delany and Lundeen, 1990) and the extended LLNL database.

The corrected equilibrium-constant data for the same temperature range, at ionic strengths of 0–2 molal and H_2S fugacities of 0–200 atm, are shown in Figure 3. Inspection of the data shows that the ionic strength has little influence on the equilibrium constant. Comparison with the original equilibrium constants in both LLNL databases reveals that they significantly underpredict H_2S solubility above 150°C at H_2S fugacities ranging from 1 to 40 atm. Duan et al. (2007) also noted that equilibrium constants calculated using the SUPCRT92 software (Johnson et al., 1992) underestimate H_2S solubility above 150ºC. At 50 atm, the LLNL data underpredict solubility across the entire temperature range, whereas at higher fugacities of 100–200 atm both LLNL databases underpredict H_2S solubility below 100ºC.

As a final step, the equilibrium constants describing the HS^- and H^+ partitioning were corrected in the LLNL database. The solubility data for dissolved H_2S and vapour-phase H_2S are given by the following two reactions:

$$H_2S(aq) = H^+ + HS^- \quad (2)$$

$$H_2S(g) = H^+ + HS^- \quad (3)$$

Given that HS^- and H^+ partitioning data for the P-T-x_{NaCl} range of the solubility model from Duan et al. (2007) are not available, it is not possible to quantify equilibrium constants for these reactions. As reaction (1) is simply reaction (3) subtracted from reaction (2), the LLNL database was modified to calculate the equilibrium constant k1 for reaction (1) from Duan et al. (2007) followed by the subtraction of k1 from k2, the equilibrium constant for reaction (2). This yields k3, the equilibrium constant for reaction (3), which was used to replace the existing values in the LLNL database.

Following correction of the equilibrium-constant data, the LLNL database was used for modelling of the present study. It is important to note that the database is configured for modelling at 1 atm, temperatures of 0–300ºC and activities calculated according to the B-dot equation of Helgeson et al. (1969) and Helgeson and Kirkham (1974). The 1 atm steam-saturation limitation appears somewhat troublesome given that seafloor hydrothermal venting occurs at a confining pressure corresponding to the hydrostatic pressure at a water depth of several hundreds to thousands of metres. However, Duan et al. (2007) pointed out that the fugacity coefficient of H_2S in the vapour phase of H_2S-H_2O mixtures differs little from that of pure H_2S within the temperature range of the model. As long as fluid temperature and hydrostatic confining pressure are below the two-phase curve for seawater (Bischoff and Rosenbauer, 1984), H_2S solubility can be estimated from H_2S fugacity apart from the saturation pressure of H_2O. Ohmoto (1996) showed that the two-phase curve of seawater is indeed an important control on the formation of modern, seafloor massive-sulphide accumulations. An additional constraint on modelling is imposed by the fact that the LLNL database is valid only for solutions with ionic strengths of up to 3.0 molal if Na and Cl are the dominant solutes. This condition is met in the case of most chloride waters sampled from modern seafloor vent sites (cf. Hannington et al., 2005).

Models of Sulphide Precipitation in Modern Vent Analogues

The quality of the equilibrium-constant data calculated above was evaluated by modelling sulphide precipitation from chloride waters of known compositions, which were sampled at modern seafloor vent sites. For this purpose, the

comprehensive compilation of modern seafloor fluid compositions by Hannington et al. (2005) was used. Although the database provides vent-fluid compositions for about 60 active vent sites worldwide, only 12 chloride waters were chosen for the present study. Most chloride waters either had temperatures exceeding the limits of the solubility model (227ºC) by Duan et al. (2007) and the LLNL thermochemical database (300ºC) or were not analyzed for all parameters required for geochemical modelling. In addition, the higher temperature vent fluids are likely poor analogues as sulphide and sulphosalt deposition at Eskay Creek occurred largely at temperatures below 200ºC (Sherlock et al., 1999). The compositions of the 12 representative modern seafloor chloride waters are summarized in Table 1. Their pH values and contents of total dissolved solids are plotted in Figure 4.

The 12 chloride waters represent four different tectonic settings, including mid-ocean ridges, sedimented ridges, ridge-hotspot intersections and back-arc spreading centres and/or rifts; the latter is probably closest to the tectonic setting of the Eskay Creek deposit. Table 1 shows that the pH of the hydrothermal fluids broadly correlates with plate-tectonic setting and generally decreases from sedimented ridges (pH = 5.0–6.0), to ridge-hotspot intersections (pH = 4.0–4.5), mid-ocean ridges (pH = 3.0–4.0) and back-

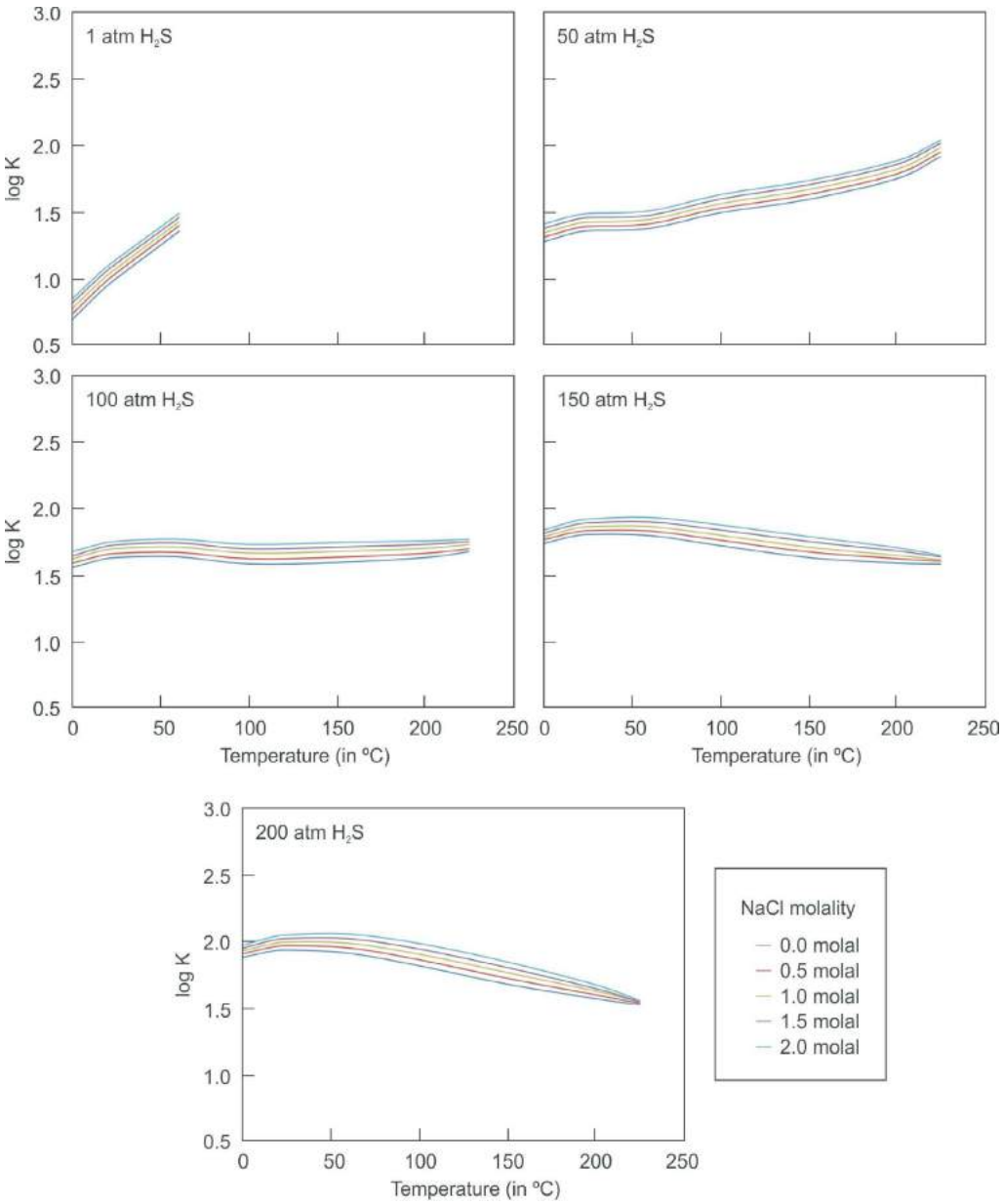

Figure 3. Temperature dependency of the equilibrium-constant K for the reaction $H_2S(aq) = H2S(g)$ at five selected H_2S fugacities and ionic strengths (NaCl molality) ranging from 0 to 2.0 molal (calculation is based on Duan et al., 2007).

Table 1. Composition of representative chloride waters from modern seafloor vent sites located in different tectonic settings (data compilation from Hannington et al., 2005).

	Seawater	North Cleft (NC) Mid-ocean ridge	South Cleft (SC) Mid-ocean ridge	21°N, EPR (EP) Mid-ocean ridge	17°S, SEPR (SE) Mid-ocean ridge	Guaymas (GY1) Sedimented ridge	Guaymas (GY2) Sedimented ridges
Temperature (°C)	2	262	224	273	300	291	285
pH (25°C)	7.8	2.8	3.2	3.8	3.1	5.9	5.9
Total dissolved solids (mg/kg)	33183	87410	73900	44697	27318	46376	49474
Ionic strength (M)	0.6144	1.53	1.307	0.7591	0.4518	0.7799	0.8392
Composition:							
Cl (mM)[1]	541	1245	1087	579	323	589	637
Fe (μM)	<0.001	16400	18739	871	3600	49	180
Mn (μM)	<0.001	4250	3585	1002	740	222	236
Cu (μM)	<0.003	0.9	10	nd	10	nd	nd
Zn (μM)	<0.01	406	575	40	130	4	40
Pb (nM)	<0.01	1085	900	183	nd	265	653
Si (mM)	0.2	24	23	20	9	13	14
SO_4 (mM)	27.9	0.01	0.01	0.01	0.01	0.01	0.01
Mg (mM)	52.7	0.01	0.01	0.01	0.01	0.01	0.01
Na (mM)	464	924	796	510	292	478	524
K (mM)	9.8	59	52	26	13	46	37
Ca (mM)	10.2	109	96	21	12	29	42
Sr (μM)	87	348	312	97	43	184	253
Li (μM)	26	2350	1718	1033	313	954	720

[1]Concentrations are reported in M (moles), mM (millimoles), μM (micromoles) or nM (nanomoles) per kilogram (kg).
Abbreviation: nd, not detected

arc spreading centres and/or rifts (pH = 2.5–4.0). The higher pH of the chloride waters from sedimented ridges is likely a reflection of the neutralizing capacity of the sedimentary hostrocks. Figure 5 shows that the Zn and Pb concentrations for ten of the vent samples (data for two samples are either missing or below detection limit) are generally inversely proportional to pH, suggesting that the more acidic fluids have a higher capacity for transporting metals.

One representative chloride water sample from each of the four tectonic settings, generally representing a median content of total dissolved solids, was selected for numerical

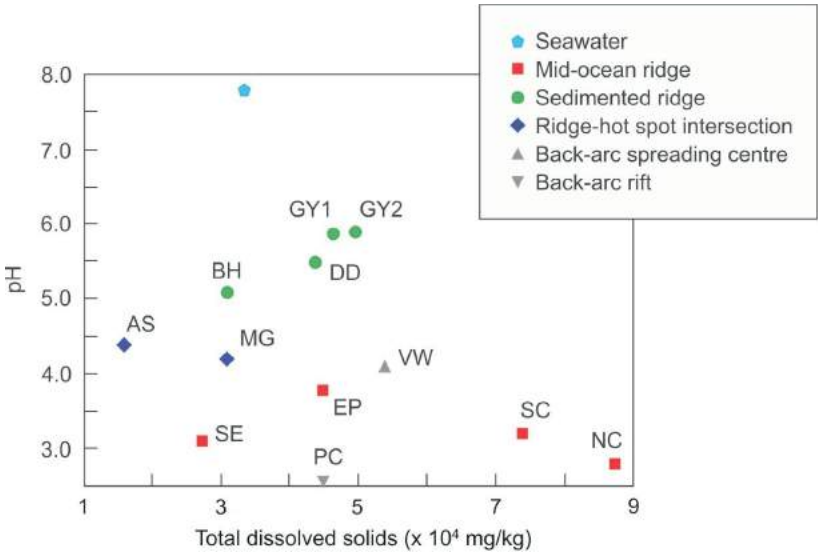

Figure 4. Scatter diagram of acidity (pH at 25°C) versus contents of total dissolved solids for representative chloride waters collected from different modern seafloor vent sites (data from Hannington et al., 2005). The composition of seawater is given for comparison. Abbreviations: AS, Axial Seamount; BH, Bent Hill; DD, Dead Dog; EP, 21ºN, EPR; GY, Guaymas; MG, Menez Gwen; NC, North Cleft; PC, Pacmanus; SC, South Cleft; SE, 17ºN, SEPR; VW, Vienna Wood.

Table 1 (continued)

	Dead Dog (DD)	Bent Hill (BH)	Axial Seamount (AS)	Menez Gwen (MG)	Vienna Wood (VW)	Pacmanus (PC)
	Sedimented ridge	Sedimented ridge	Ridge-hotspot intersection	Ridge-hotspot intersection	Back-arc spreading centre	Back-arc rift
Temperature (°C)	276	265	299	284	282	268
pH (25°C)	5.5	5.1	4.4	4.2	4.1	2.6
Total dissolved solids (mg/kg)	43530	30763	15593	30881	54010	44723
Ionic strength (M)	0.7361	0.5325	0.243	0.5155	0.9138	0.7446
Composition:						
Cl (mM)[1]	578	412	176	380	712	572
Fe (μM)	20	17	12	28	109	2404
Mn (μM)	63	78	142	59	348	3116
Cu (μM)	1.3	0.3	0.7	2.7	2	36
Zn (μM)	1.7	0.7	2.3	4.2	10	115
Pb (nM)	125	50	191	nd	4	7000
Si (mM)	10	nd	14	10	15	16
SO_4 (mM)	0.01	0.01	0.01	0.01	0.01	0.01
Mg (mM)	0.01	0.01	0.01	0.01	1	0.01
Na (mM)	398	315	148	313	534	445
K (mM)	19	14	7	23	24	86
Ca (mM)	81	40	10	32	82	15
Sr (μM)	257	162	46	110	290	97
Li (μM)	500	370	184	270	1010	724

modelling. The four sites chosen were South Cleft (mid-ocean ridge), Dead Dog (sedimented ridge), Menez Gwen (ridge-hotspot intersection), and Pacmanus (back-arc rift). The four modelled vent fluids were speciated and cooled via simple, polythermal reaction-path models at fixed H_2S fugacities (constrained by aqueous-H_2S concentrations of the vent fluids) using The Geochemist's Workbench® software (Bethke, 2008) and the LLNL thermochemical database, modified using H_2S-solubility corrections from Duan et al. (2007) at discrete pressures of 5–200 atm. Figure 6 shows an example output for one of the reaction-path models.

Modelling showed that the chalcopyrite mineral-solubility data in the LLNL database yielded incorrect results. Consequently, data from the MINTEQ database (Allison et al., 1991) was used. As H_2S-solubility data calculated according to Duan et al. (2007) are only slightly affected by

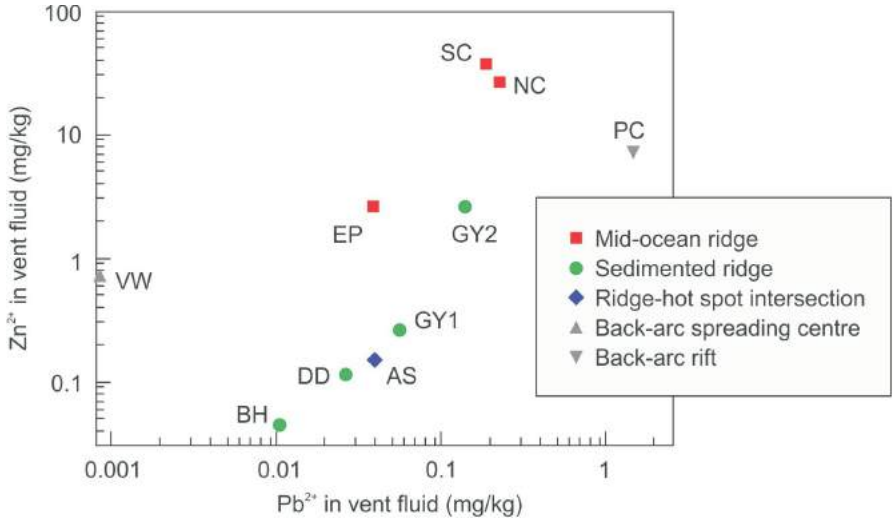

Figure 5. Scatter diagram of Zn versus Pb for representative chloride waters collected from different modern seafloor vent sites (data from Hannington et al., 2005). Abbreviations: AS, Axial Seamount; BH, Bent Hill; DD, Dead Dog; EP, 21ºN, EPR; GY, Guaymas; NC, North Cleft; PC, Pacmanus; SC, South Cleft; VW, Vienna Wood.

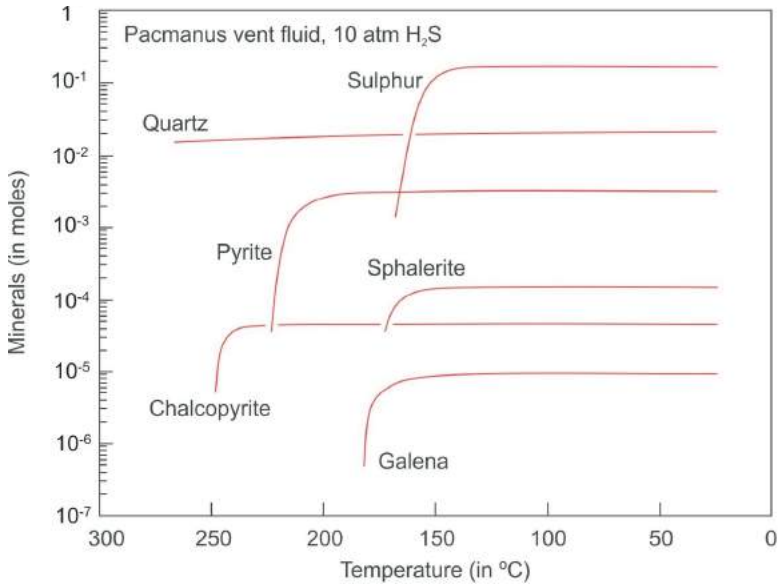

Figure 6. Results of a polythermal reaction-path model using The Geochemist's Workbench® software (Bethke, 2008) for chloride waters from the Pacmanus vent site. Chalcopyrite precipitation was modelled using thermodynamic data from the MINTEQ database (Allison et al., 1991). All other sulphides are modelled using data from the Lawrence Livermore National Laboratory database.

changes in ionic strength, a mid-range ionic strength of 1.0 molal (total dissolved solids of 55 g/kg) was chosen so that only H_2S corrections for temperature and pressure required evaluation. Figure 7 shows calculated dissolved H_2S concentrations at 1.0 molal ionic strength for discrete temperatures between 0 and 300ºC, using the modified LLNL datasets at pressures between 5 and 200 atm. Solubility data above the temperature limit (227ºC) of the model by Duan et al. (2007) and above boiling temperatures and below the boiling pressures were estimated using polynomial-trend fits.

Measured dissolved H_2S concentrations of the four vent fluids ranged from 0.0016 molal at Menez Gwen to 0.0068 molal at Pacmanus. Figure 7 can be applied to estimate H_2S fugacity using dissolved-H_2S concentrations and vent temperatures (the plot cannot be used to estimate mineralization depth as H_2S fugacity is independent of water-saturation pressure). In addition, there is a high uncertainty in the H_2S-solubility curves at high temperatures and low pressures, as solubility curves in this region contain extrapolated data. Nonetheless, first-order estimates suggest H_2S fugacities of 10–20 atm at South Cleft, and of 30–40 atm at Dead Dog, Menez Gwen and Pacmanus.

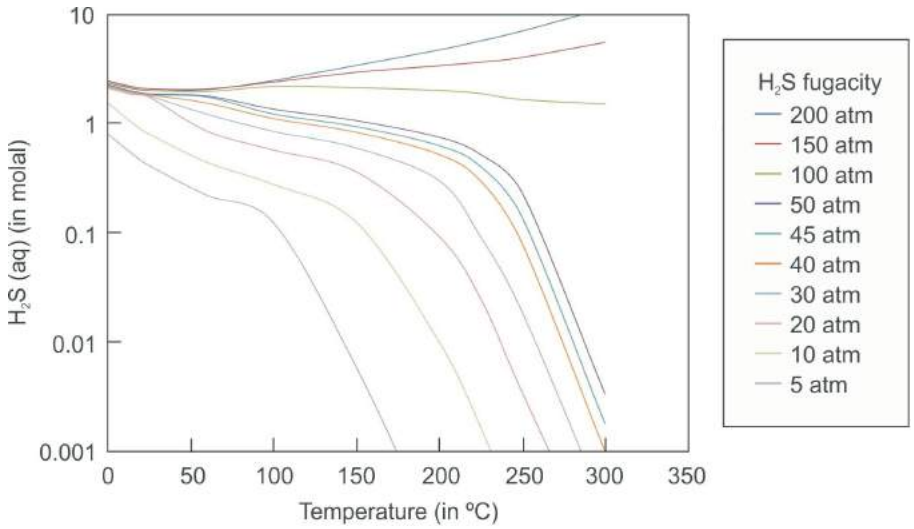

Figure 7. The H_2S-solubility data derived from the model presented in Duan et al. (2007) plotted as a function of temperature for different H_2S fugacities.

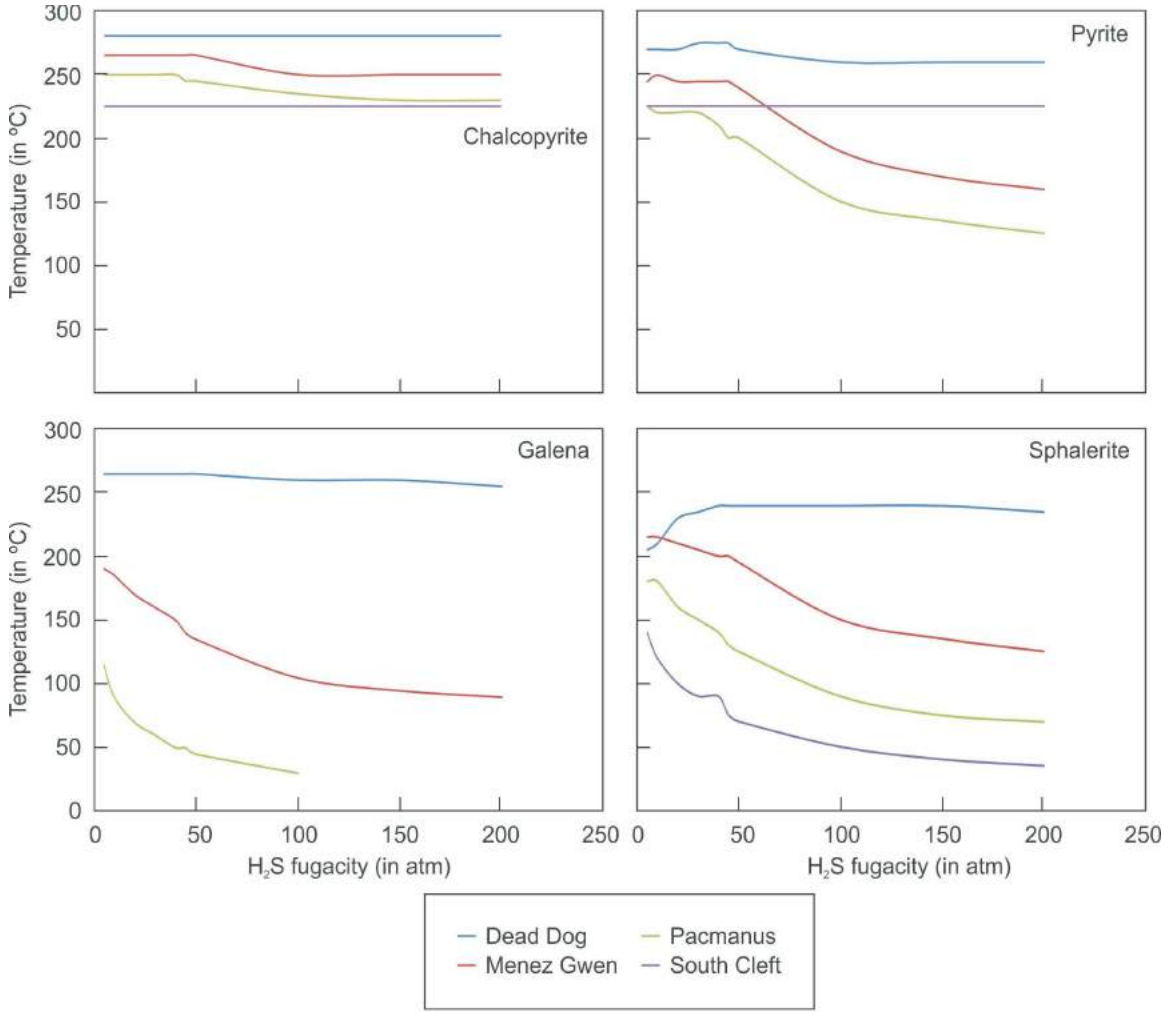

Figure 8. Temperatures of first precipitation of chalcopyrite, pyrite, galena and sphalerite for chloride waters sampled from the South Cleft, Dead Dog, Menez Gwen and Pacmanus vent sites at a range of H_2S fugacities.

Figure 8 shows the temperatures of first precipitation of chalcopyrite, pyrite, galena and sphalerite for H_2S fugacities ranging from 5 to 200 atm. In general, precipitation temperatures are proportional to fluid pH, with near-neutral fluids from Dead Dog precipitating sulphides at the highest temperatures, whereas the chloride waters at South Cleft and Pacmanus precipitate sulphides at distinctly lower temperatures (Table 2). The calculated sulphide-precipitation temperatures conform closely to observations made on the modern seafloor (cf. Hannington et al., 2005).

Homogenization temperatures of fluid inclusions in sphalerite from Eskay Creek range up to 180–220ºC (Sherlock et al., 1999). Modelling of the present study suggests that a fluid with a pH of 4.0–5.0 is necessary to generate sphalerite at these temperatures (assuming that the homogenization temperatures are similar to the temperatures of formation). The crossover pH between CO_2 dissolved in chloride waters and the generation of bicarbonate waters is approximately 4.5 at 200ºC (Bischoff and Rosenbauer, 1996). This suggests that a fluid with a pH somewhat higher

Table 2. Calculated sulphide-precipitation temperatures for four representative modern seafloor vent sites.

Vent site	Water depth (m)	Fluid temperature (ºC)	pH	$fH_2S(g)$ (atm)	Calculated sulphide-precipitation temperature (ºC)			
					Chalco-pyrite	Pyrite	Galena	Sphalerite
South Cleft	2300	224	3.2	10–20	224	224	80	130
Dead Dog	2425	276	5.5	30–40	276	276	265	235
Menez Gwen[1]	850	284	4.2	30–40	265	245	–	200
Pacmanus	1650	268	2.6	30–40	250	215	155	135

[1] Fuid does not contain Pb.

than that of the chloride waters from Menez Gwen would be capable of reaching carbonate saturation under those conditions, which would have been critical for generating the carbonate-kaolinite alteration halo at Eskay Creek. Although the hydrothermal fluids venting at Pacmanus represent the closest modern analogue to the mineralizing fluids at Eskay Creek in terms of tectonic setting and local host-rock composition, the numerical modelling shows that the alkalinity and pH of the chloride waters venting at Pacmanus are too low to explain the formation of the carbonate-kaolinite alteration halo observed at Eskay Creek. This alteration must have been caused by a bicarbonate water of higher alkalinity and near-neutral pH.

Future Modelling Work

The present modelling, largely based on thermochemical data from the LLNL database, successfully evaluated the role of simple cooling on sulphide precipitation in seafloor hydrothermal vents of different compositions. Predicted sulphide-precipitation temperatures closely conformed to seafloor observations, indicating that the data of Duan et al. (2007) provide a reliable approximation of H_2S solubility. Modelling of the present study also showed that chalcopyrite-solubility data from the MINTEQ dataset (Allison et al., 1991) is more reliable than that from the LLNL database. Future modelling will evaluate whether MINTEQ data are also more appropriate to describe solubility for other sulphide phases commonly precipitating at seafloor hydrothermal vents.

Following adequate description of sulphide precipitation, geochemical modelling will focus on the formation of the carbonate-kaolinite alteration at Eskay Creek, which represents for exploration the most useful vector to mineralization. This will require a better understanding of the controls on carbonate solubility, which is a direct function of dissolved and vapour-phase CO_2 concentrations. Similar to the H_2S-solubility data, CO_2 solubility in most thermochemical databases is currently only parameterized at low pressures and temperatures. To overcome this problem, the CO_2-solubility model of Duan and Sun (2003) and Duan et al. (2006), which is accurate over geologically relevant temperatures, pressures and fluid-solute levels, will be implemented using the approach established in this paper.

Once H_2S and CO_2 solubility in the mineralizing hydrothermal fluids is correctly described over the relevant pressure and temperature ranges, geochemical modelling will be able to show whether simple interaction with the wallrock and simple cooling of the chloride waters forming the sulphide and sulphosalt mineralization at Eskay Creek could have resulted in the generation of the bicarbonate waters responsible for the formation of the carbonate-kaolinite alteration. Future model calculations will also explore an alternative hypothesis that involves the effervescence of CO_2 from the chloride waters at higher temperatures, coupled with the subsequent take-up of the CO_2 by cooler, ambient pore waters, possibly producing waters of sufficient alkalinity and near-neutral pH to form the carbonate-kaolinite alteration halo.

Acknowledgments

The authors gratefully acknowledge the financial support provided by Geoscience BC, Barrick Gold Corporation, the Michael-Jürgen-Leisler-Kiep Foundation and the German Research Foundation. This study would not have been possible without the help provided by T. Roth, M.D. Hannington and R. Tosdal. R. Kleeberg is thanked for providing analytical support.

References

Alldrick, D.J., Nelson, J.L., Barresi, T., Stewart, M.L. and Simpson, K. (2005): Geology of the Upper Iskut River area, British Columbia; BC Ministry of Energy and Mines, Open File 2006-2, scale 1: 100 000.

Allison, J.D., Brown, D.S. and Novo-Gradac, K.J. (1991): User's manual for MINTEQA2/PROFEFA2, version 3.0: a geochemical assessment model for environmental systems; United Stales Environmental Protection Agency, Environmental Research Laboratory, 107 p.

Barrett, T.J. and Sherlock, R.L. (1996): Geology, lithogeochemistry and volcanic setting of the Eskay Creek Au-Ag-Cu-Zn deposit, northwestern British Columbia; Exploration and Mining Geology, v. 5, p. 339–368.

BC Geological Survey (2011): MINFILE BC mineral deposits database; BC Ministry of Energy and Mines, URL <http://www.empr.gov.bc.ca/Mining/Geoscience/MINFILE/Pages/default.aspx> [November 2011].

Bethke, C.M. (2008): Geochemical and Biogeochemical Reaction Modeling; Cambridge University Press, New York, 543 p.

Bischoff, J.L. and Rosenbauer, R.J. (1984): The critical point and two-phase boundary of seawater, 200°–500°C; Earth and Planetary Science Letters, v. 68, p. 172–180.

Bischoff, J.L. and Rosenbauer, R.J. (1996): The alteration of rhyolite in CO_2 charged water at 200 and 350°C: the unreactivity of CO_2 at higher temperature; Geochimica et Cosmochimica Acta, v. 60, p 3859–3867.

Britton, J.M., Blackwell, J.D. and Schroeter, T.G. (1990): #21 zone deposit, Eskay Creek, northwestern British Columbia; BC Ministry of Energy and Mines, Exploration in British Columbia 1989, p. 197–223.

Childe, F. (1996): U-Pb geochronology and Nd and Pb isotope characteristics of the Au-Ag rich Eskay Creek volcanogenic massive sulfide deposit, British Columbia; Economic Geology, v. 91, p. 1209–1224.

Delany, J.M. and Lundeen, S.R. (1990): The LLNL thermochemical database; Lawrence Livermore National Laboratory, Report URCL-21658, 150 p.

Duan, Z., Møller, N. and Weare, J.H. (1996): Prediction of the solubility of H_2S in NaCl aqueous solution: an equation of state approach; Chemical Geology, v. 130, p. 15–20.

Duan, Z. and Sun, R. (2003): An improved model calculating CO_2 solubility in pure water and aqueous NaCl solutions from

273 to 533 K and from 0 to 2000 bar; Chemical Geology, v. 193, p 257–271.

Duan, Z., Sun, R., Zhu, C. and Chou, I.M. (2006): An improved model for the calculation of CO_2 solubility in aqueous solutions containing Na^+, K^+, Ca^{2+}, Mg^{2+}, Cl^-, and SO_4^{2-}; Marine Chemistry, v. 98, p. 131–139.

Duan, Z., Sun, R., Liu, R. and Zhu, C. (2007): Accurate thermodynamic model for the calculation of H_2S solubility in pure water and brines; Energy and Fuels, v. 21, p. 2056–2065.

Ettlinger, A.D. (1992): Hydrothermal alteration and brecciation underlying the Eskay Creek polymetallic massive sulphide deposit; *in* Geological Fieldwork 1991, BC Ministry of Energy and Mines, Paper 1992-1, p. 535–541.

Gabrielse, H., Monger, J.W.H., Wheeler, J.O. and Yorath, C.J. (1991): Morphogeological belts, tectonic assemblages and terranes; *in* Geology of the Cordilleran Orogen in Canada, H. Gabrielse and C.J. Yorath (ed.), Geological Survey of Canada, Geology of Canada, no. 4, p. 15–28 (also Geological Society of America, Geology of North America, v. G-2).

Hannington, M.D., Poulsen, K.H., Thompson, J.F.H. and Sillitoe, R.H. (1999): Volcanogenic gold in the massive sulfide environment; Reviews in Economic Geology, v. 8, p. 325–356.

Hannington, M.D., de Ronde, C.E.J. and Petersen, S. (2005): Seafloor tectonics and submarine hydrothermal systems; Economic Geology, 100th Anniversary Volume, p. 111–141.

Helgeson, H.C., Garrels, R.M. and Mackenzie, F.T. (1969): Evaluation of irreversible reactions in geochemical processes involving minerals and aqueous solutions–II. Applications; Geochimica et Cosmochimica Acta, v. 33, p. 455–481.

Helgeson, H.C. and Kirkham, D.H. (1974): Theoretical prediction of the thermodynamic behavior of aqueous electrolytes at high pressures and temperatures, II. Debye-Huckel parameters for activity coefficients and relative partial molal properties; American Journal of Science, v. 274, p. 1199–1261.

Johnson, J.W., Oelkers, E.H. and Helgeson, H.C. (1992): SUPCRT92: a software package for calculating the standard molal thermodynamic properties of minerals, gases, aqueous species, and reactions from 1 to 5000 bar and 0 to 1000ºC; Computers and Geosciences, v. 18, p. 889–947.

Large, R.R. (1977): Chemical evolution and zonation of massive sulfide deposits in volcanic terrains; Economic Geology, v. 72, p. 549–572.

Meuzelaar, T. and Monecke, T. (2011): Carbonaceous mudstone hosting the Eskay Creek deposit (NTS 104B/09, /10), northwestern British Columbia: multivariate statistical analysis of compositional trends; *in* Geoscience BC Summary of Activities 2010, Geoscience BC, Report 2011-1, p. 45–56.

Monecke, T., Gale, D., Roth, T. and Hannington, M.D. (2005): The submarine volcanic succession hosting the massive sulfide and sulfosalt Eskay Creek deposit, Canada; *in* Mineral Deposit Research: Meeting the Global Challenge, Y. Mao and F.P. Bierlein (ed.), Proceedings of the 8th Biennial SGA (Society for Geology Applied to Mineral Deposits) Meeting, August 18–21, 2005, Beijing, Peoples Republic of China, Springer, p. 655–658.

Nadaraju, G.D. (1993): Triassic–Jurassic biochronology of the eastern Iskut River map area, northwestern British Columbia, M.Sc. thesis, University of British Columbia, 268 p.

Ohmoto, H. (1996): Formation of volcanogenic massive sulfide deposits: the Kuroko perspective; Ore Geology Reviews, v. 10, p. 135–177.

Pitzer, K.S. (1973): Thermodynamics of electrolytes–I. Theoretical basis and general equations; Journal of Physical Chemistry, v. 77, p. 268–277.

Robinson, H.M. (1991): Mineralisation and alteration patterns of the Central Lens (21B Zone), Eskay Creek, British Columbia, Canada; M.Sc. thesis, Imperial College, University of London, 129 p.

Roth, T., Thompson, J.F.H. and Barrett, T.J. (1999): The precious metal-rich Eskay Creek deposit, northwestern British Columbia; Reviews in Economic Geology, v. 8, p. 357–373.

Schardt, C., Cooke, D.R., Gemmell, J.B. and Large, R.R. (2001): Geochemical modeling of the zoned footwall alteration pipe, Hellyer volcanic-hosted massive sulfide deposit, western Tasmania, Australia; Economic Geology, v. 96, p. 1037–1054.

Sherlock, R.L., Roth, T., Spooner, E.T.C. and Bray, C.J. (1999): Origin of the Eskay Creek precious metal-rich volcanogenic massive sulfide deposit: fluid inclusion and stable isotope evidence; Economic Geology, v. 94, p. 803–824.